Chapter 1

Background Information

The densification of particles to strengthen a conglomerate by heating has been done for thousands of years to produce pottery and bricks. Sintering is the process of transforming a powder into a solid body using heat. Solid state diffusion allows materials with very high melting temperatures to reach a full density below their melting point and retain small grain sizes. The application of sintered parts to modern engineering practices and problems allows the field to advance. Research and development of sintering processes aim to produce materials faster, more controllably, and with superior properties.

1.1 Sintering

A simple illustration of the sintering process is shown in figure 1.1 where two initially spherical particles move together and become one volume:

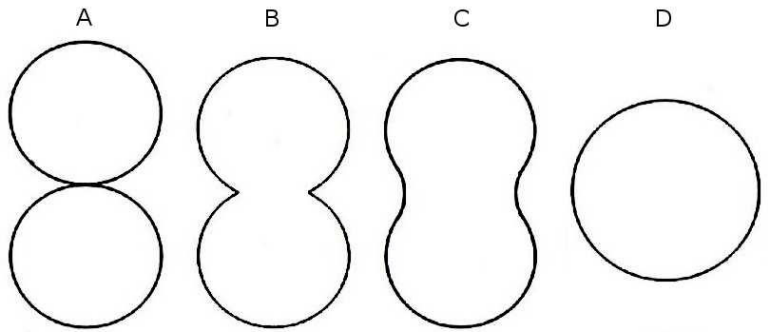

Figure 1.1: Sintering in a two particle system. A) Initial loose powder, very small neck between particles B) early stages of neck formation C) intermediate stage of neck formation D) Fully sintered particle [2]

The solid state diffusion of atoms brings the particle centers closer together. In a large array of particles, the surface area is reduced along with the volume of pores.

1.1.1 General diffusion

The diffusion equation can be derived from conservation of mass. The change in concentration φ with time is equal to the flux of material, J, flowing in and out of that volume:

$$\frac{\partial \varphi}{\partial t} = \nabla \cdot J \tag{1.1}$$

Fick's first law models the natural flux of a species due to a variable concentration. The magnitude of the flux is linearly proportional to the concentration gradient and is scaled by the diffusion rate D:

$$J = -D\nabla\varphi \tag{1.2}$$

Combining these two equations leads to the general diffusion equation:

$$\frac{\partial \varphi}{\partial t} = \nabla \cdot [-D\nabla\varphi] \tag{1.3}$$

In one dimension:

$$\frac{d\varphi}{dt} = -D\frac{d^2\varphi}{dx^2} \tag{1.4}$$

The diffusion coefficient is a function of temperature and can be modeled by the Arrhenius equation:

$$D = D_o \exp\left(-\frac{Q}{RT}\right) \tag{1.5}$$

Where D_o is a coefficient, Q is the activation energy, and R is the gas constant.

1.1.2 Diffusion mechanisms in sintering

Powders are inherently in an unstable state. Generally, the reduction of surface free energy (by eliminating pores) provides the driving force for densification. All surfaces have a free energy associated with their radius of curvature. The equilibrium condition for a particle is given by the energy balance:

$$\sigma dV + \gamma dA = 0 \tag{1.6}$$

where σ is the surface stress due to the curvature and γ is the surface energy. Assuming the particle is a sphere, the differentials dA and dV in terms of the radius r of the sphere are:

$$\begin{aligned} dA &= 8\pi r dr \\ dV &= 4\pi r^2 dr \end{aligned} \tag{1.7}$$

combining these equations:

$$\sigma = \gamma \frac{8\pi r dr}{4\pi r^2 dr} = \gamma \frac{2}{r} \tag{1.8}$$

And the principal curvatures r_1 and r_2 that define a 3D surface:

$$\sigma = \gamma \left(\frac{1}{r_1} + \frac{1}{r_2}\right) \tag{1.9}$$

When the powder is heated to high temperatures, the system is allowed significant atomic motion. Mass is rearranged in order to reduce the free surface energy due to this curvature.

Mass transport pathways are shown in figure 1.2 and table 1.1

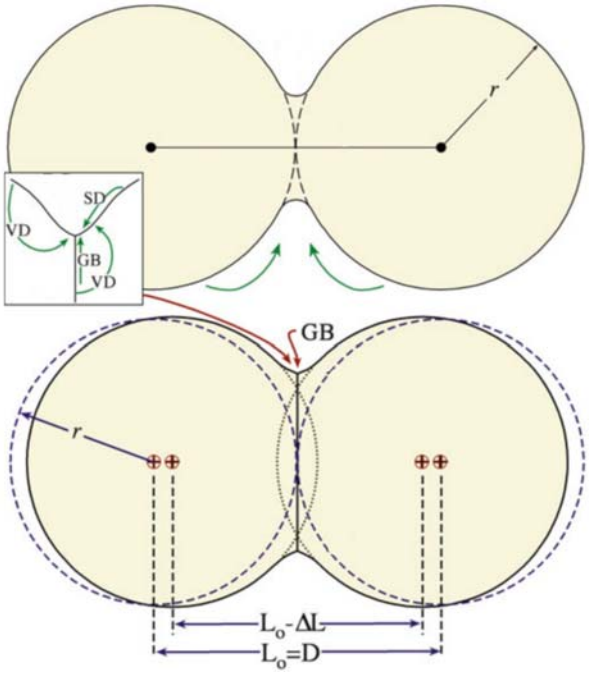

Figure 1.2: Sintering of two sphere model showing mass diffusion pathways to the neck leading to densification [3]

Table 1.1: Diffusion pathways during sintering leading to densification

Mechanism	*Transport path*	*Source*
SD	Surface diffusion	Surface
VD	Volume diffusion	Surface
GD	Grain boundary diffusion	Grain boundary
VD	Volume diffusion	Grain boundary

Sintering shrinkage appears as a sigmoidal curve that can be broken up into three density ranges, ρ, each associated with a specific microstructure. The densification curves shown in figure 2.4 illustrates typical behavior.

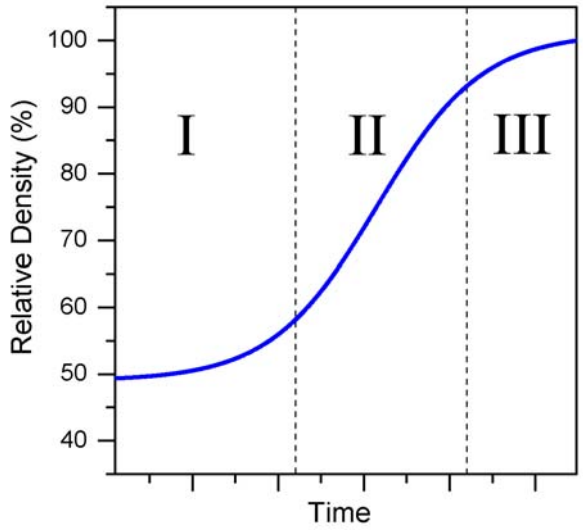

$\rho_g \lesssim$ Stage I $\lesssim 55\%$
$55\% \lesssim$ Stage II $\lesssim 90\%$
$90\% \lesssim$ Stage III $\lesssim 100\%$

Figure 1.3: The stages of sintering. Stage II is roughly defined as the linear section of the sigmoidal densification curve.

Surface diffusion

Stage I sintering is characterized by rapid growth of inter-particle necks. The macroscopic shrinkage of the sample during stage I is negligible. Surface diffusion is the primary mass transport mechanism at low temperatures [4]. Microstructures held at stage I temperatures long enough will coarsen as shown in figure 1.4. The curvature in the powder body is reduced without densification. Surface diffusion (as well as evaporation-condensation) therefore competes against densifying mechanisms to reduce the surface free energy due to curvature.

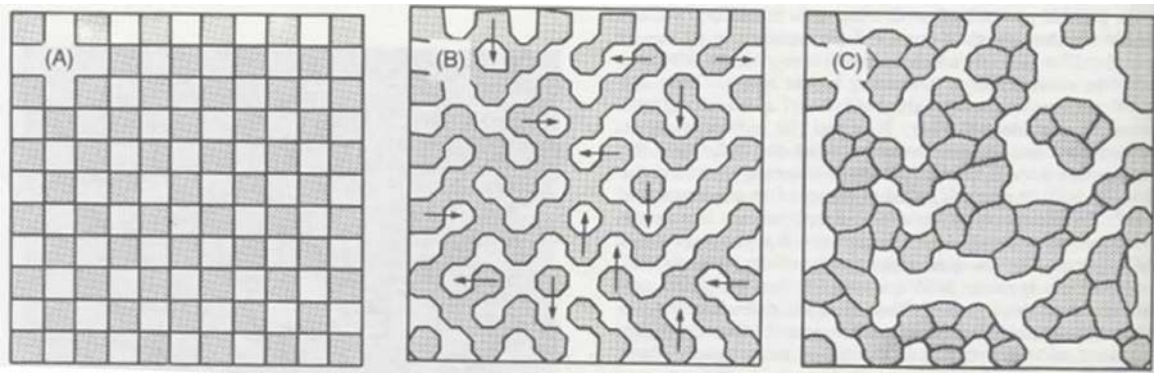

Figure 1.4: Reduction of surface curvature in a microstructure coarsening due to surface diffusion [5]

The crystalline nature of materials can often be seen by the formation of facets on the grain surface. Figure 1.5 shows facets on an Al_2O_3 grain after extended time spent at stage I temperatures.

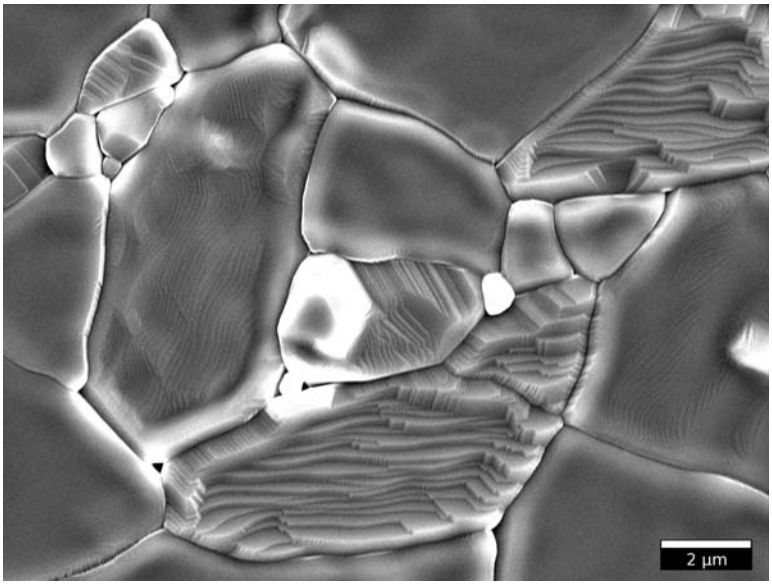

Figure 1.5: Facets on the surface of an Al_2O_3 grain after free sintering in air.

Volume diffusion

Stage II sintering is characterized by the middle (linear) section of the sigmoidal densification curve. Volume diffusion and grain boundary diffusion are primarily responsible for this densification.

Volume diffusion involves the motion of vacancies through the volume of the particle. The equilibrium concentration of vacancies increases with temperature. There are three main vacancy diffusion pathways through the volume of the grain that contribute to sintering. The vacancy flow (and atomic flow in the opposite direction) involves free surfaces, grain boundaries and dislocations.

Vacancies created on the neck surface at grain boundary move through the bulk volume then annihilate on the free surface. This is effectively surface transportation and does not contribute to densification.

Vacancies created on the neck surface move to and annihilate on the grain boundary. This deposits atoms on the grain boundary and allows the neck to grow, bringing the particle centers closer together [3]. Reference figure 1.2 to visualize the pathways atoms take due to this motion, note that vacancy motion is opposite the arrows in the figure. In materials that are compressed prior to densification (as in SPS and hot pressing) the dislocations due to plastic deformation can significantly contribute to densification early during sintering. The dislocations move to annihilate on the neck surface and densification occurs because the vacancy source is not a surface.

Grain boundary diffusion

Mass flows along the grain boundary and is redeposited at the neck surface. The atoms brought to neck surface are then redistributed around the particles by surface diffusion. Grain boundaries

form between the individual particles due to misaligned crystal structures. As the surface curvature is reduced at higher densities, grain boundary equilibrium becomes important.

Combined stage sintering model

Researchers Hansen, et al., developed the "combined stage-sintering model" which equates the measured densification to the contribution of volume and grain boundary diffusion [1]:

$$-\frac{1}{L}\frac{dL}{dt} = \frac{\gamma\Omega}{kT}\left(\frac{\Gamma_V D_V}{G^3} + \frac{\Gamma_B D_B}{G^4}\right) \tag{1.10}$$

Where the normalized instantaneous linear shrinkage, $\frac{1}{L}\frac{dL}{dt}$, is proportional to the grain size G of the particles, D_V, D_B are the diffusion rates, Γ_V, Γ_B are geometric scaling terms associated with volume and grain boundary diffusion respectively. Ω is the atomic volume, k is the Boltzmann constant.

For isotropic shrinkage, the linear shrinkage rate can be converted to densification by:

$$-\frac{1}{L}\frac{dL}{dt} = \frac{d\rho}{3\rho dt} \tag{1.11}$$

1.2 Master Sintering Curve

Combing the diffusion terms, D_V and D_B, in equation 1.10 to a single Arrhenius equation, the densification rate becomes:

$$\frac{d\rho}{3\rho dt} = \frac{\gamma\Omega}{kT}\frac{\Gamma(\rho)D_o}{G(\rho)^n}\exp\left(-\frac{Q_{MSC}}{RT}\right) \tag{1.12}$$

With this assumption, the densification occurs due a single transport mechanism associated with an activation energy Q_{MSC} which is defined as the *apparent sintering activation energy*. The exponent n is associated with either volume or grain boundary diffusion. This assumes that G and λ are only functions of density. Equation 1.12 can be rearranged and integrated:

$$\int_0^t \frac{1}{T} \exp\left(-\frac{Q_{MSC}}{RT}\right) dt = \frac{k}{\gamma \Omega D_0} \int_{\rho_0}^{\rho} \frac{G(\rho)^n}{3\rho\Gamma(\rho)} d\rho \tag{1.13}$$

The right hand side of this equation includes all of the mass transport processes produced by the sintering environment. The left hand side is an easily computed integral of the heating schedule:

$$\Theta(t,T) \equiv \int_0^t \frac{1}{T} \exp\left(-\frac{Q_{MSC}}{RT}\right) dt \tag{1.14}$$

If a specific powder is sintered with several different heating schedules and the dominate mass transport mechanism remains constant, then the plot of each densification pathway and $\Theta(t,T)$ resolve to a single locus defined as the Master Sintering Curve (MSC) shown in figure 1.6 [6]. The MSC derivation assumes a single dominate densification mechanism and pressureless isotropic shrinkage.

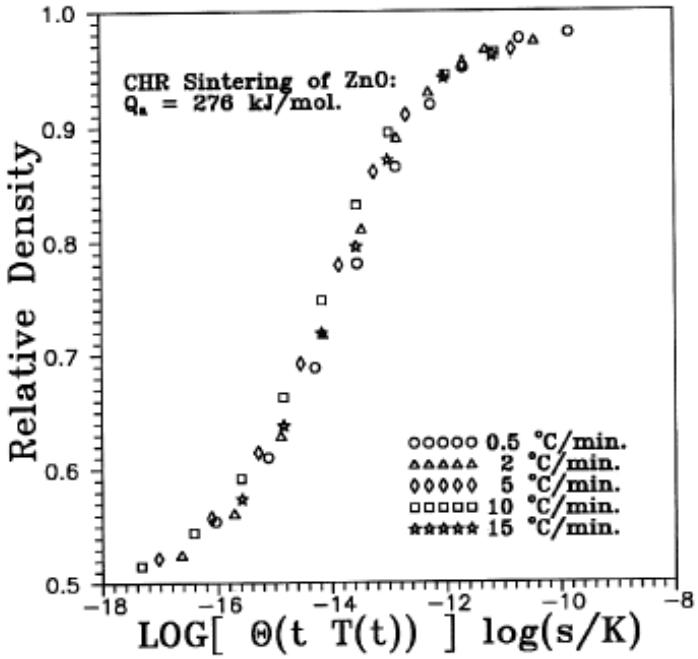

Figure 1.6: The Master Sintering Curve from five different thermal schedules [6]

Literature typically calculates the MSC using the shrinkage measured in $50\% < \rho < 90\%$. In a brute force calculation, the $\Theta(t, T)$ term is calculated for each heating schedule over a range of possible Q_{MSC}. The difference between the $\Theta(T(t))$ term at each density is summed and defined as MRS, Mean Residual Square:

$$MRS = \sqrt{\frac{1}{\rho_f - \rho_g} \int_{\rho_g}^{\rho_f} \frac{\sum_{i=1}^{N} (\Theta_i / \Theta_{avg} - 1)^2}{N} d\rho} \tag{1.15}$$

Where N is the number of heating schedules, Θ_i / Θ_{avg} is the ratio of that single heating schedule Θ to the average value of all Θ at that density.

The MRS minimum is shown graphically in figure 2.2 where Q_{MSC} produces the lowest MRS. This method is widely used in the literature as a useful tool to easily develop densification models from experimental data.

MSC with applied loads

While the MSC method was derived using equations of grain boundary and volume diffusion, ignoring plastic flow densification mechanisms, researchers showed that MSC method remains applicable in pressure assisted densification [7]. They sintered alumina using five different heating schedules at five different applied loads. They created a pressure-assisted master sintering surface which allowed them to predict density to 1% accuracy shown in figure 1.7.

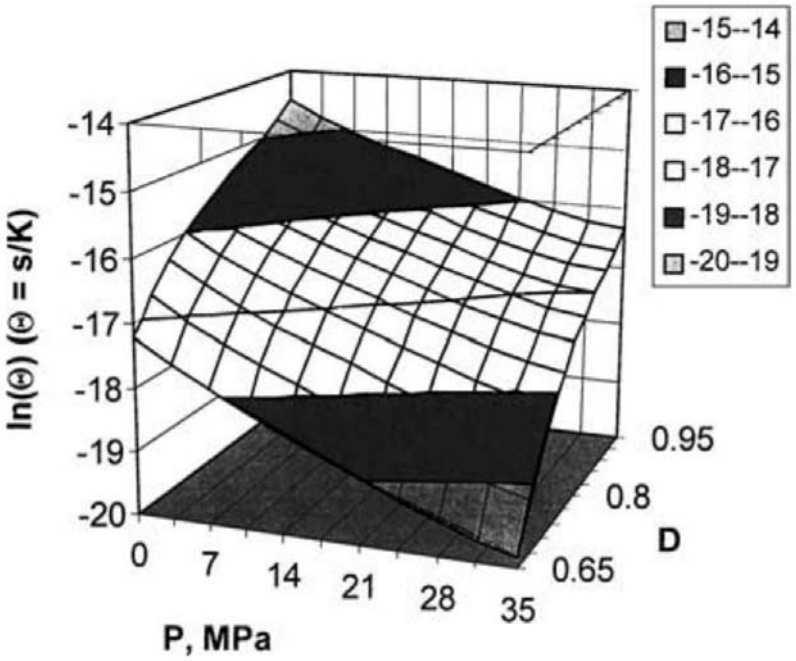

Figure 1.7: The pressure-assisted master sintering surface developed from five thermal schedules at a range of pressures applied pressured [7]

Guillon and Langer showed how equation 1.12 can be modified to include an applied pressure. They then used the pressure assisted MSC method to successfully model densification with an electric field [8].

The applied load can be larger than the sintering stress but not large enough to activate excessive plasticity. This means the dominant densification mechanism is a diffusional process. Volume

diffusion processes may increase the shrinkage rate because of an increased number of dislocations forming in the the volume of the particle. The dislocations form vacancies that diffuses to the grain boundary which causes shrinkage. The axial strain rate is then:

$$\frac{d\rho}{3\rho dt} = \frac{\gamma\Omega}{kT}\frac{\Gamma(\rho)D_o}{G(\rho)^n}\exp\left(-\frac{Q_{MSC}}{RT}\right)[\phi(\rho)p_a]^m \tag{1.16}$$

The terms in the square brackets include the effect of added pressure where ϕ is the stress intensification factor as function of density, p_a is the applied load, and m is a diffusion exponent (m=1) for grain boundary and volume diffusion. This equation is rearranged as before to:

$$\int_0^t \frac{1}{T}\exp\left(-\frac{Q_{MSC}}{RT}\right)dt = \frac{k}{3\gamma\Omega D_0 p_a^m}\int_{\rho_0}^{\rho}\frac{G(\rho)^n}{\rho\Gamma(\rho)\phi(\rho)^m}d\rho \tag{1.17}$$

This pressure assisted MSC equation has the same $\Theta(t,T)$ term as before and is used in the same way. Their calculated MSC model used heating rates 35, 50, 100, 150 K/min on alumina with 50 MPa applied load. Their model was within 1% of a $75K/min$ heating rate sintered in the same way.

1.3 Spark Plasma Sintering

Spark Plasma Sintering (SPS) or Electric Field Assisted Sintering (EFAS) is a technique where powders are compressed by a uniaxial load inside resistively heated graphite tooling. The discharge of an electric current through the graphite allows very fast heating schedules compared to conventional hot-pressing or free sintering. Less time spent at low temperatures can reduce microstructural coarsening [9] and the applied electric field can lower the energy required for mass

transport [10]. A typical research size (20 mm diameter punch and die) SPS graphite tooling stack is shown in figure 1.8.

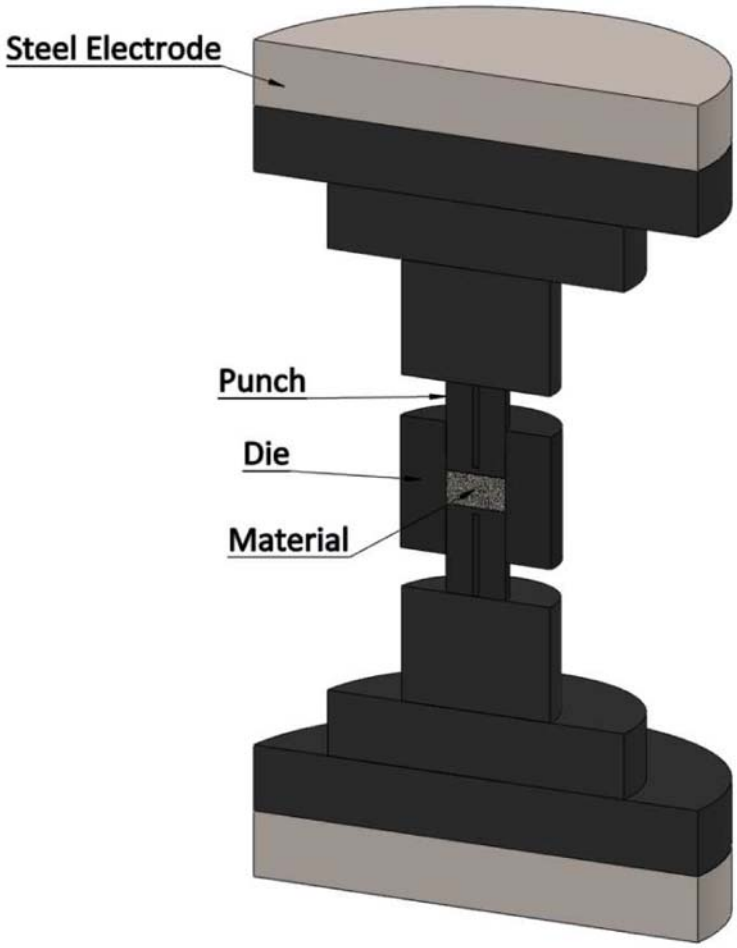

Figure 1.8: The cross-section of a typical SPS graphite stack and water cooled steel electrodes of sintering machine

The SPS samples used in this study are heated at $\sim 150^oC/min$ to a desired maximum temperature. The current $I(t)$ controlled by a thermocouple in a PID feedback loop:

$$\begin{aligned} I(t) &= K_p(T_{PID}) + K_I \int_0^t T_{PID} dt + K_d \frac{d}{dt} T_{PID} \\ T_{PID} &= T_{desired} - T_{measured} \end{aligned} \tag{1.18}$$

The proportion-integral-derivative feedback loop equation is a function of T_{PID}, which is the difference between the desired temperature defined by the heating schedule and the measured temperature at the thermocouple probe. The coefficients K_P, K_I, K_D are numerical values that tune the response behavior.

Temperature measurement must be carefully considered in SPS. As shown by the temperature distribution on a cross-section of a standard die and punch in figure 1.9, the location of the temperature probe should be very near the sample to avoid erroneous measurements. Large temperature differences between the outside diameter surface and the powder body exists, as well as along the length of the punches.

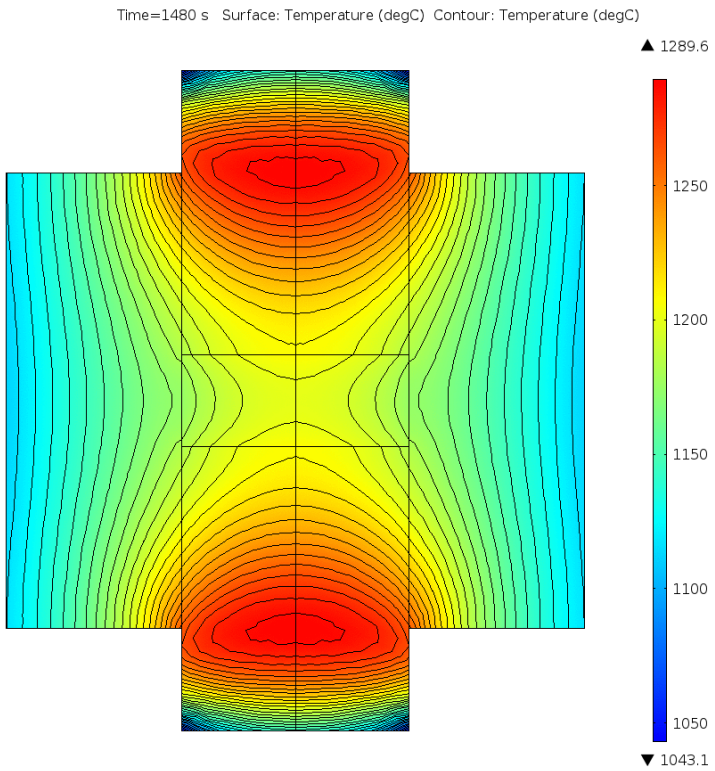

Figure 1.9: Temperature distribution in standard SPS die during heating with standard thermal boundary conditions mentioned in section 2.1

The current supplied by the SPS capacitor bank used in this study (Fuji-SPS Model 3.20) is a pulsed DC wave form. Electric fields induce interesting effects on ionic ceramic diffusion characteristics, and EFAS is a very active field of research to understand and measure the effects. In SPS, the application of an electric field from as low as 2 V/cm has been shown to significantly reduce grain growth in 3% yttria-stabilized zirconia (3YTZ) [11]. Researchers made the 3YTZ samples with 60 nm average grain size and 99% density. They annealed samples under at 1300^oC for 10 hours under no voltage, 1.3 V/cm, 3.3 V/cm, 8.3 V/cm and 11.3 V/cm. The sample without an electric field reached an average grain size of $210 \pm 10nm$. The samples heated with an electric field had a 15% - 40% reduction in grain size as shown by figure 1.10.

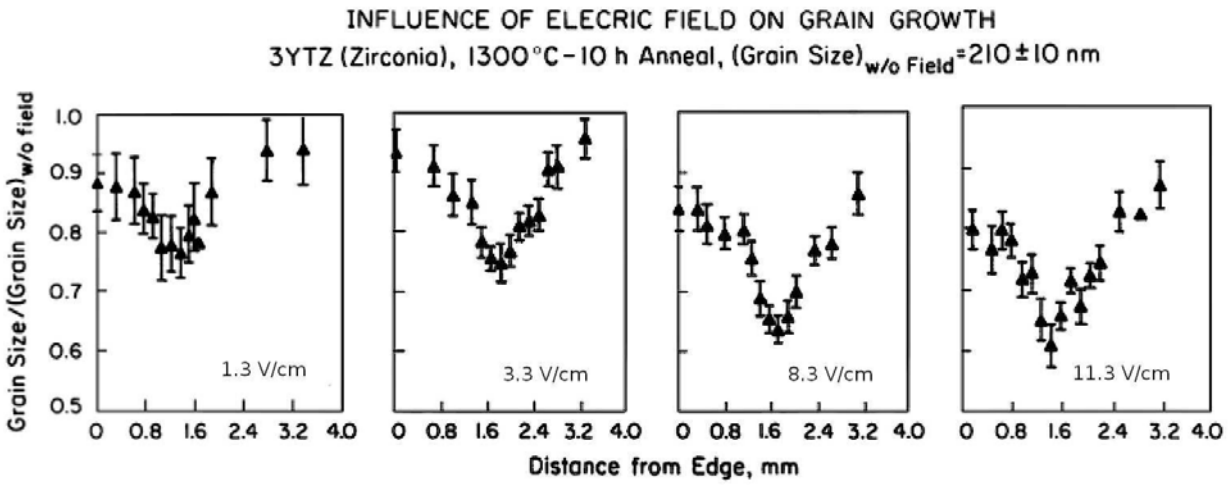

Figure 1.10: The grain size of samples annealed at high temperature with an electric field, relative to the grain size from a sample without an electric field. The field strength reported in bottom of each graph is valid at the grain size minimum. The field is variable across the sample due to the electrode configuration. The applied electric field is inversely proportional to grain size. [11]

The direction of the applied electric field has also been shown to influence the grain boundary migration [12]. Starting with $0.2\mu m$ average size 99.99% pure Al_2O_3 powder, the researchers sintered and annealed the samples to a grain size of $170\mu m$. They polished a surface with $1\mu m$

diamond paste. Then the same powder was placed on the polished surface and hot-pressed to full density with a grain size of approximately $4\mu m$.

Samples were annealed at 1600^oC for 2 hours with no field, with a 200 V/cm field positive on the large grain side and positive on the small grain side. The grain migration from the original interface (visible by a planar array of pores) was $6\mu m$ with no field, $\sim 3-4\mu m$ with positive voltage on the large grain side, and $\sim 12-15\mu m$ with positive voltage on the small grain side.

Depending on the electric field direction, the diffusion coefficient of the rate limiting species can be increased significantly [13]. The enhanced diffusion rate of ionic ceramics due to an electric fields as well the capability of fast heating rates make electric field assisted sintering (EFAS) well apt to quickly sinter high temperature ceramics to full density with small grain sizes. Additionally, the reconfigurability of temperatures within EFAS tooling make it a promising method to create new and useful materials.